



ELSEVIER

Available online at [www.sciencedirect.com](http://www.sciencedirect.com)

ScienceDirect

journal homepage: [www.elsevier.com/locate/he](http://www.elsevier.com/locate/he)

# Electrochemically etched triangular pore arrays on GaP and their photoelectrochemical properties from water oxidation

Changqing Zhu, Maojun Zheng\*, Zuzhou Xiong, Hong Li, Wenzhong Shen

Key Laboratory of Artificial Structure and Quantum Control, Ministry of Education, Department of Physics and Astronomy, Shanghai Jiao Tong University, Shanghai 200240, PR China

## ARTICLE INFO

### Article history:

Received 12 February 2014

Received in revised form

11 April 2014

Accepted 4 May 2014

Available online 3 June 2014

### Keywords:

Triangular pore arrays

Photoelectrochemical performance

Photocatalytic water splitting

High-field electrochemical etching

## ABSTRACT

Large-scale, triangular pore arrays on GaP were successfully prepared via a simple and high-efficient approach of electrochemical etching under high field. The obtained ordered porous GaP exhibited high performance in the photoelectrochemical (PEC) properties compared with bulk GaP. The photocurrent of the porous GaP exceeded one order of magnitude higher than that of bulk material under 0.1 V compared to the reversible hydrogen electrode (RHE), which indicated the porous structure could enhance photo-response and facilitate the separation of photo-induced carrier charges and their collection. The structure of triangular pore arrays cooperated with its depth determined the PEC performance of GaP. The optimal etching depth was obtained via testing the PEC performance. The hydrogen production from bulk GaP and its porous structure material were also tested from water splitting. Upon the porous structure, significantly enhanced hydrogen production has also been observed, which indicated that the porous GaP should have important potential in photocatalytic water splitting.

Copyright © 2014, Hydrogen Energy Publications, LLC. Published by Elsevier Ltd. All rights reserved.

## Introduction

Energy harvested from sunlight offers a reliable approach to solve the energy crisis. As the largest renewable energy source, the solar energy would provide a great possibility to solve the terawatt energy challenge. However, the sunlight is daily and seasonal variability in nature. In order to obtain a stable, constant energy flux, solar energy should be converted into chemical energy that can be efficiently used, stored, and transported upon the demand. An attractive approach is

converting solar energy into high-energy chemical bonds, such as splitting water into hydrogen by sunlight [1–4]. Theoretically, the efficiency of a single band gap system could reach up to 17%, which was assumed a 0.8 V overpotential [5]. A higher theoretical efficiency has been predicted when two semiconductors are coupled as the photoanode and photocathode to mimic natural photosynthesis [5,6].

The free energy change for the conversion of H<sub>2</sub>O molecules to H<sub>2</sub> and O<sub>2</sub> is 237.2 kJ/mol. According to the Nernst equation, it corresponds to  $\delta E = 1.23$  V per electron transferred. Therefore, the theoretical minimum band gap for the

\* Corresponding author. Tel./fax: +86 21 34202791.  
E-mail address: [mjzheng@sjtu.edu.cn](mailto:mjzheng@sjtu.edu.cn) (M. Zheng).

water splitting is 1.23 eV [1–4]. Compared to other available semiconductors, GaP is a promising photoelectrode material for the water splitting since its conduction band edge is higher than the redox potential of  $H_+/H_2$  [7–10]. However, the short carrier diffusion length in GaP leads to excessive minority carrier recombination, which limits the utilization of GaP as a photoelectrode. In order to solve this problem, several groups investigated nonplanar semiconductor heterojunction [11–16]. Moreover, much interest has been focus on the utilization of nanoarchitecture to solve this issue [17–19]. It has been reported that the photogenerated charge collection efficiencies of GaP photoelectrodes can be improved by adjusting the nonplanar photoelectrode containing nanowire, macropore, etc. [6,9,16]. Although the preparation of porous GaP has been studied extensively [20–27], the application of porous GaP on water splitting is scarce. Price et al. pointed out that the macroporous n-type GaP photoelectrodes could support both large photovoltages and photocurrents [16].

In this report, high-field electrochemical etching (i.e. high current density,  $1400 \text{ mA cm}^{-2}$ ) has been used to obtain porous GaP with regular triangular pores in our system. Through the photoelectrochemical test, including photovoltage, photocurrent and  $I-V$  curves, one can find that the porous structure obviously improves the photoelectrochemical performance, in comparison with the bulk GaP. In addition, the porous GaP is much more productive than bulk GaP for the light-induced water splitting process.

## Experimental sections

### Preparation of ordered porous GaP and characterization

Single crystalline n-GaP (111) wafer (300  $\mu\text{m}$  thick) doped with sulfur at concentration of  $4 \times 10^{17} \text{ cm}^{-3}$  was obtained from GRIM Electro-optic Materials Co., Ltd. Wafer was cut into  $8 \text{ mm} \times 8 \text{ mm}$  and degreased by successively sonicating in acetone and ethanol. And then they were rinsed with the deionized water and dried in a nitrogen stream. Indium films were deposited on the sample back surface by direct current magnetron sputtering for Ohmic contacts. Then high purity silver paint was smeared on the In films in order to establish an electric contact with a copper plate. The copper plate except the sample was painted with inert epoxy to ensure only the sample contact with the electrolyte. Then the copper plate with the sample was pressed in an O-ring of an electrochemical cell leaving the sample exposed to the electrolyte. A two-electrode set-up was used for electrochemical etching. The sample was used as the working electrode. The counter electrode was graphite electrode. Etching of planar GaP was performed in a mixture solution of 0.5 M HBr and 0.309 M oxalic acid. Prior to etching, the solution was put into water bath under  $4^\circ\text{C}$  for 30 min. In order to explore the optimization of the depth of the porous structure, the etching was performed galvanostatically at 0.9 A for 15 s, 30 s, 45 s, and 60 s, with vigorous stirring.

The etched GaP samples exhibited dark yellow and there was a compact irregular layer on the surfaces of them. The next step was to remove the irregular layer. The etched GaP samples were immersed in aqua regia (3:1 HCl/HNO<sub>3</sub> by

volume) for 180 s. As a result, the porous GaP samples were obtained and appeared bright yellow. Scanning electron microscopic analysis of these materials was conducted with an FEI Sirion 200 scanning electron microscope (SEM). The crystal structure and phase of the samples before and after etching were determined by X-ray diffraction (XRD: D8 ADVANCE X-ray diffractometer, Bruker, Germany) with Cu  $K\alpha$  radiation (1.54  $\text{\AA}$ ). The reflectance spectrum of porous GaP was measured by using a Lambda 750S spectrometer (Perkin–Elmer) consisting of a deuterium and tungsten-halogen lamp, photomultiplier, and integrating sphere with 60 mm. The samples were placed at the end of the sphere at normal incidence. The reflection measurements on the triangular pore arrays are normalized by the reflection of the bulk GaP to obtain the relative reflectance of the porous GaP.

### Photoelectrochemical tests

Photoelectrochemical analyses under white light illumination were conducted using an online acquisition system. Photovoltage measurements of bulk GaP and porous GaP electrodes were performed using a three-electrode configuration, with GaP materials as the working electrode, platinum gauze as the counter electrode, and saturated Ag/AgCl as the reference electrode. A mixture solution of 0.35 M Na<sub>2</sub>S and 0.25 M Na<sub>2</sub>SO<sub>3</sub> was used as the electrolyte, and it played a role of the photo-induced hole scavenger and its pH was 13.35. An electrochemical workstation (PARSTAT 4000) instrument was used to measure open-circuit photovoltage characteristics of the electrode. The illuminated area of the working electrode was  $0.64 \text{ cm}^2$ . A 300 W Xe lamp (SOLARDGE 700, Beijing Perfectlight Technology Co. Ltd, China) was used as the light source. The power intensity of the light was  $400 \text{ mW cm}^{-2}$ , which was measured by Solar Simulator Spectroradiometer (LS-100, EKO Instruments Co., Ltd, Japan).

The chronoamperometry measurement of  $I-t$  photo-response was evaluated under the same illumination at an applied potential of 0.1 V contrast to the RHE. The current–voltage ( $I-V$  curves) was also obtained to indicate the characteristics of the electrode with a scan rate of 0.1 V/s. The measured potentials versus the Ag/AgCl reference electrode were converted to the RHE scale through the following calculation  $E_{\text{RHE}} = E_{\text{Ag/AgCl}} + 0.059\text{pH} + E^{\circ}_{\text{Ag/AgCl}}$  [28],  $E^{\circ}_{\text{Ag/AgCl}}$  is the standard potential of Ag/AgCl at  $25^\circ\text{C}$  (0.1976 V). For incident photon to current efficiency (IPCE) measurement, the monochromatic irradiation from a Xe lamp equipped with bandpass filters (central wavelengths: 450 nm and 550 nm), and the photocurrent was recorded at a constant bias 0.1 V vs. RHE.

The apparatus for water splitting was a gas-closed circulation system (Beijing Perfectlight Technology Co. Ltd, LabSolar-IIIAG) including a vacuum line and a reaction cell with a top window Pyrex cell and this system connect with the gas chromatograph (GC). The amount of evolved H<sub>2</sub> was analysed at the online gas chromatograph (Shanghai Tech-comp Scientific Instrument Co. Ltd., D7900P) included MS-5A column and a thermal conductivity detector (TCD), and N<sub>2</sub> was the carrier gas.

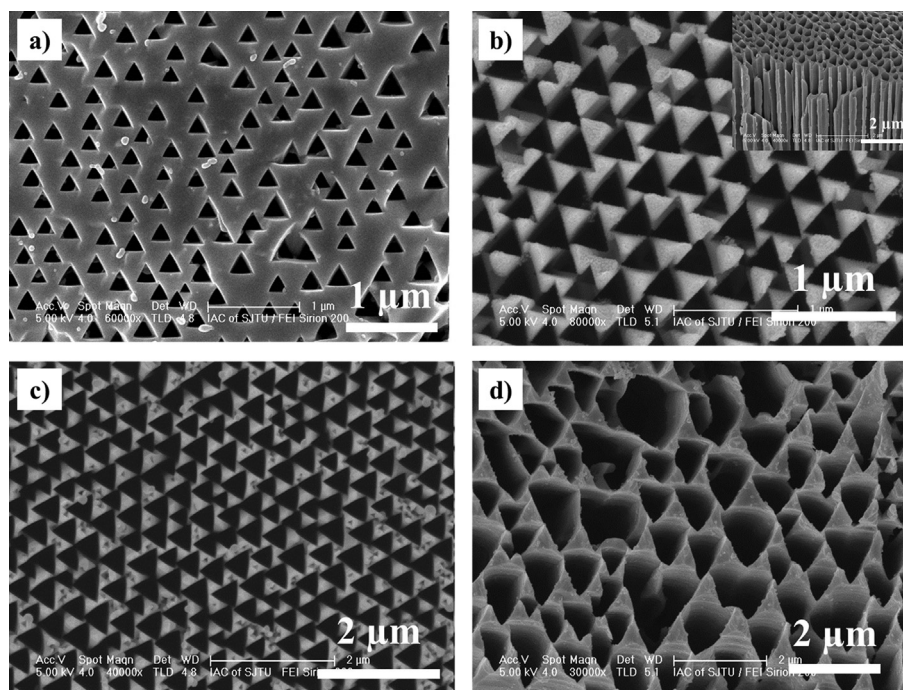


**Fig. 1** – Triangular porous arrays of GaP with different etching time. (a) SEM image of the porous structure under the etching time 15 s. (b) The morphology of porous GaP with the etching time 30 s. The inset was its corresponding cross section. (c) Under the etching time 45 s, the pore size was increasing over time. (d) The pore began to be destroyed under the etching time 60 s.

## Results and discussions

The morphology of the porous GaP with different etching time was shown in Fig. 1. When the etching time was 15 s, there were lots of triangle pore arrays and the average pore size was about 215 nm as illustrated in Fig. 1a. In Fig. 1b, large area triangle pore arrays appeared and the average pore size was about 300 nm. During the 30 s etching time, the depth of pores can reach to 35  $\mu\text{m}$ . The etching velocity is about  $1.2 \mu\text{m s}^{-1}$ . The cross section of the triangular pores can be seen in the inset of Fig. 1b. Under the etching time of 45 s and 60 s, the morphology of porous GaP was given in Fig. 1c and d, respectively. One can identify that the porous GaP own the triangular pore and straight pores with regular distribution. Thus, the large scale of ordered porous GaP has been completed by high-efficient process under high field. In addition, one can find that the average pore size will be larger as the etching time increases. Fig. 2 showed the variation between pore size and etching time. It is worth noting that when the etching time exceeds 60 s, parts of the pore wall began to vanish, namely, the triangular pore arrays have been destroyed.

XRD patterns obtained from the GaP material before and after etching (Fig. 3) matched that of zinc blend GaP (JCPDS Card 32-0397). The position of each peak was the same for all samples, indicating no change of lattice constant for the GaP before and after etching.

The mechanism of the ordered porous GaP can be explained based on the control of defect and crystal

orientation. During the electrochemical etching, an irregular layer formed on the top of ordered porous arrays, which could be contributed to the defect control. The further etching originated from the initial pore and propagated in all direction radially away from the primary surface imperfection [20,29–31]. When the irregular layer was completed, the regular triangle began to form under the mutual effect of crystal orientation and high current density. The sidewalls of ordered porous GaP are parallel to the  $\langle 111 \rangle$  crystal orientation. The triangular symmetry suggested that the sidewall is (110) surface, which is the most stable crystallographic plane in the zinc blende structure. The stability of crystal orientation

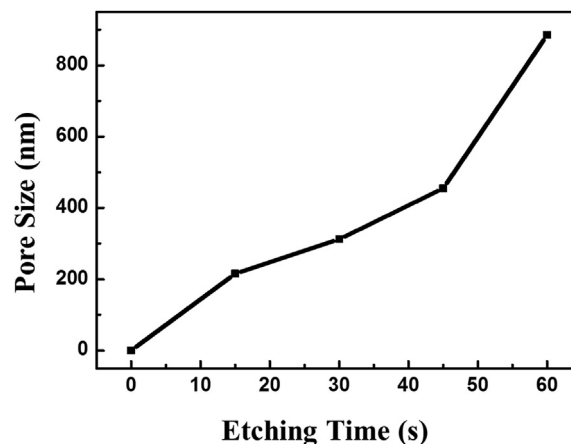


**Fig. 2** – The variation of pore size with etching time.

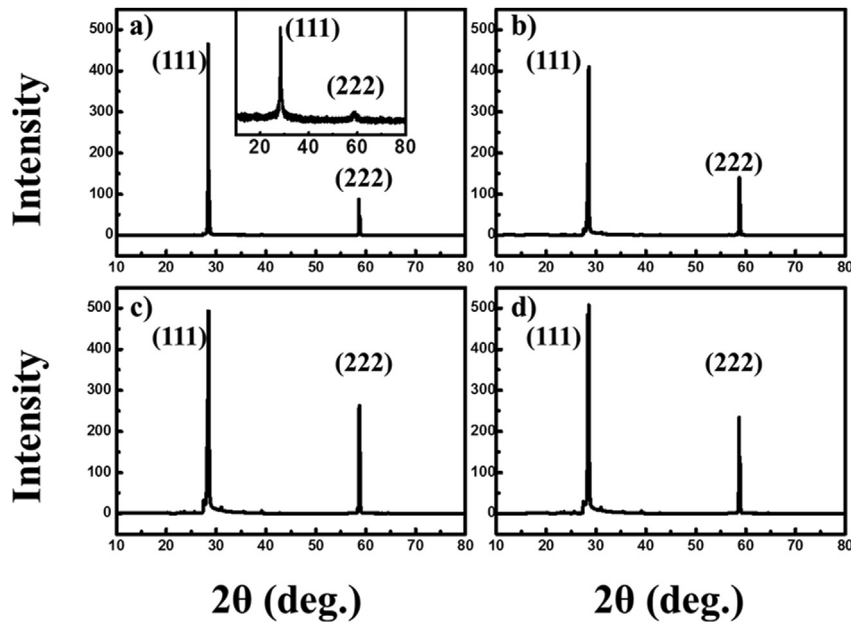


**Fig. 3** – X-ray diffraction pattern for bulk GaP and porous GaP with different etching time. (a) The XRD pattern of porous GaP with etching time 15 s. The inset corresponded to the XRD pattern of bulk GaP. (b), (c) and (d) were XRD patterns of porous GaP with etching time of 30 s, 45 s, and 60 s, respectively.

played an important role during the formation of pores. The growth mechanism of porous structure was investigated in view of crystal orientation [25,31–34]. The formation of triangular pores has been studied by Müller et al in detail. For the bulk GaP, the crystal planes (100) and (111), as there exist dipole moments to be perpendicular the surfaces, are less stable than the surface (110) [24]. Thus during the electrochemical etching, the (100) and (111) surfaces are easier to be etched.

The photovoltage was measured as the difference of open-circuit potential between dark and illumination. Fig. 4a showed the open-circuit photovoltage of the porous GaP and bulk GaP. On average, the photovoltage of ordered porous GaP (140 mV) was twice as large as that of bulk GaP (70 mV), which may be attributed to the decrease of carrier charge recombination or the geometry that significantly enhanced light absorption in the ordered porous structure because of the photovoltage formed between the semiconductor/liquid junction [1,6,35]. Fig. 4b showed the total reflectance spectra of the ordered porous GaP compared with the bulk GaP material, it can be seen that the porous GaP possessed more light absorption than the bulk material in the range of 300–500 nm, which was mainly to absorb photon to promote the electron from the valence band to conduction band. This further confirmed the above speculation. Another noticeable feature in Fig. 4b was that the 45 s etched sample possessed lower reflectance than other time etched samples in 300–450 nm, therefore it trapped much light absorption in this range.

Fig. 5 showed the energy band schematic of the contact between the semiconductor and solution. When the contact reached balance in the dark,  $qV_b$  is the barrier height as shown in Fig. 5b, which determines the theoretical limitation of the photovoltage. Introducing the light in this system, the band

bending will vary along with the various concentrations of electron and hole producing the corresponding Fermi level. The difference between the Fermi level of dark and illumination determines the photovoltage. The light intensity will affect the width of band bending to change the magnitude of the photovoltage. The magnitude of photovoltage determines the reactions of a PEC system and its analytical equation for the photovoltage formed at the contact of semiconductor/liquid is given by [15,16]

$$V_{oc} = n \frac{k_B T}{q} \ln \left( \frac{J_{ph}}{\chi J_s} \right) \quad (1)$$

where  $n$ ,  $k_B$  and  $T$  are the diode quality factor, Boltzmann's constant and temperature, respectively.  $J_{ph}$  is the photocurrent density, which is produced under illumination.  $\chi$  represents the ratio of the actual area of junction to the geometric surface of the electrode.  $J_s$  is the saturation current density.

The open-circuit voltage will reduce along with increasing the junction surface area of a semiconductor photoelectrode through nano-structuring, which has been demonstrated. However, this reduction can be compensated under the case that much more light was absorbed [15,36]. Compared with both photovoltage of the porous and planar electrode, there was much higher photocurrent in the porous than the bulk material, which indicated the effect of photocurrent is larger than the impact of the  $\chi$  in the photovoltage measurement. As for the ordered porous GaP, besides the enhanced light absorption, these could also be contributed that the porous structure owned smaller depletion and larger band bending than the bulk materials [35]. As the photovoltage is the potential at which the net collected current is zero, the recombination will lower the photovoltage [37–42]. In contrast to the bulk material, the porous structure can enhance the

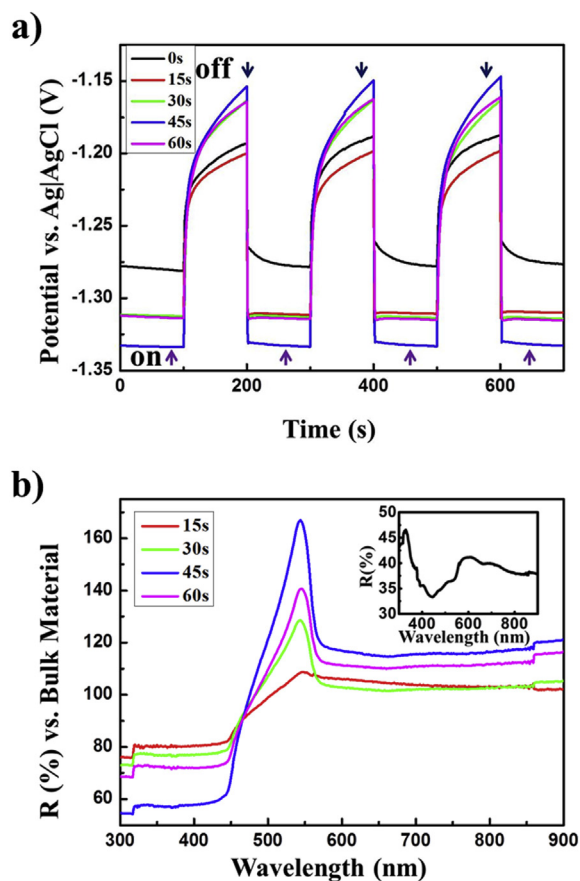
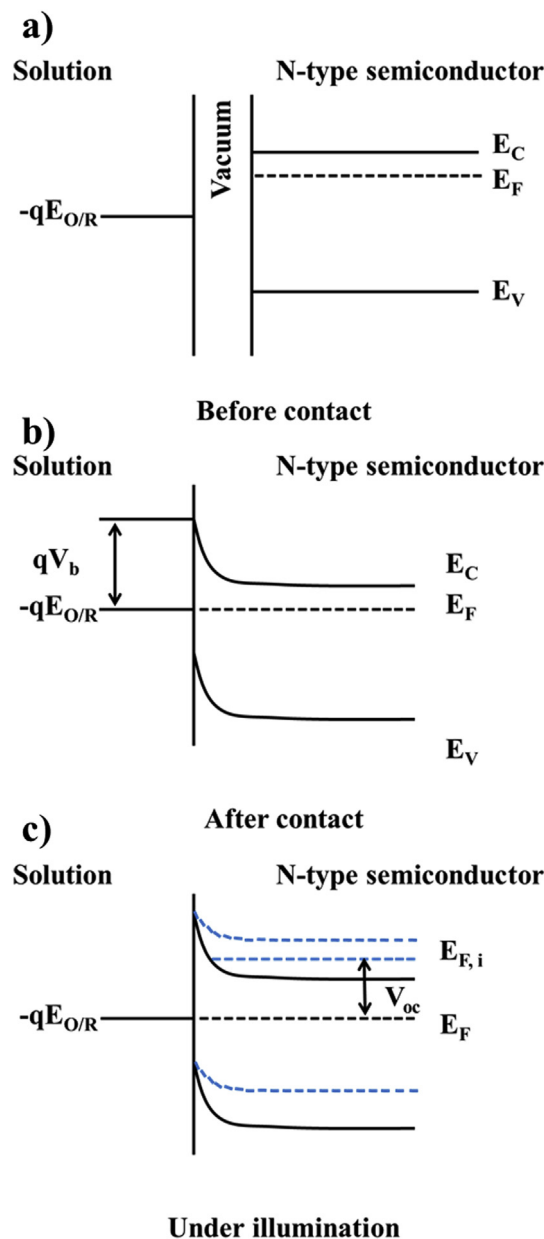


**Fig. 4** – (a) Photoelectrochemical open-circuit photovoltage of porous GaP and the corresponding bulk material. The illumination was turned on and off with a period of 100 s. (b) The relative reflectance spectrum of the porous GaP compared with the bulk material. The inset was the reflectance spectrum of the bulk GaP.

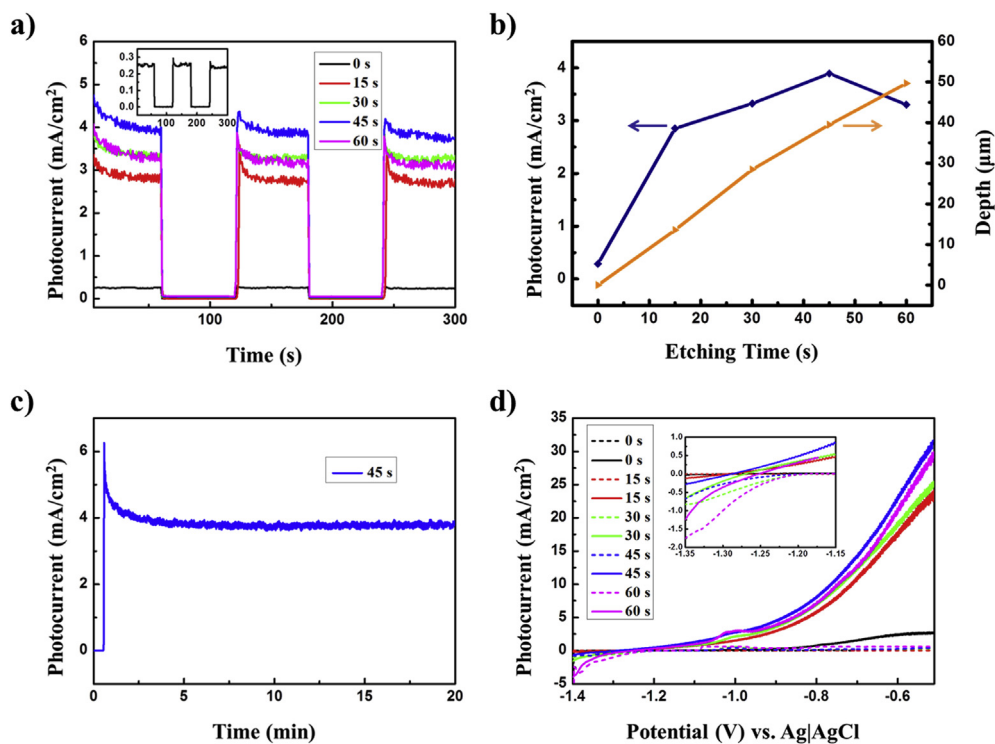
photocurrent collection and reduce the carrier charge recombination, which can also be demonstrated in the measurement of photocurrent.

Fig. 6a showed the chronoamperometry measurement of bulk GaP and porous GaP with different etching time under 0.1 V in contrast to  $V_{RHE}$ . The bulk GaP was marked as 0 s. The photocurrent density of the porous structure photoelectrode was over one order of magnitude higher than that of the bulk photoelectrode. This indicated that the porous GaP structure is much more beneficial for the charge carrier transportation than the bulk GaP. On one hand, a narrower band-bending region represents a stronger electric field close to the interface of semiconductor/liquid, producing higher charge separation efficiency and photocurrent density. The photocurrent of porous GaP would be improved with increasing the etching time as shown in Fig. 6a about curves marked 0 s, 15 s, 30 s, and 45 s. However, when the etching time was 60 s, there was a reduction. Under the observation of SEM, it was found that the partial walls of triangular pores etched with 60 s began to vanish, which results in the formation of larger pores, and the walls of pores were much thinner than the sample with etching time 45 s. Fig. 6b showed the correlation of depth and

photoresponse with the etching time. One can find that the optimal etching time is 45 s, which corresponds to the maximum photocurrent, which demonstrates that the triangular pore structures and etching depth both enhance the photoresponse for indirect semiconductors [43]. In the bulk photoelectrode, the thickness of the bulk material should be large enough to ensure efficient light absorption. While the minority carriers have to travel a long distance before reaching the surface to complete the water oxidation, which results in the low efficiency of the photoelectrode. In contrast, the porous structure allows the light to be absorbed efficiently



**Fig. 5** – The formation process of the photovoltage between semiconductor and electrolyte. (a) The energetic band schematic before the contact. (b) The case of after contact, but in the dark. (c) Under illumination, the band bending decrease and the Fermi level moved to the flat-band potential.



**Fig. 6** – (a) Chronoamperometry measurement (at 0.1 V vs. RHE) of porous GaP and the bulk material. The illumination was turned on and off with a period of 60 s. The inset was the corresponding photoresponse of bulk GaP. (b) The correlation of photocurrent (blue) and pore depth (yellow) with different etching time. The photocurrent data was measured at 0.1 V versus RHE. (c) Time courses for the photocurrent of porous GaP etched time with 45 s. (d) Linear scan voltammetry measurements of porous GaP and the corresponding bulk GaP. All experiments were performed with the mixture electrolyte solution of 0.25 M  $\text{Na}_2\text{SO}_3$  and 0.35 M  $\text{Na}_2\text{S}$  (pH = 13.35). (For interpretation of the references to colour in this figure legend, the reader is referred to the web version of this article.)

along their entire length, while holes can diffuse to the surface over a short distance along the pore path. Large surface area and efficient carrier collection is promoted to complete the water splitting. Therefore, the ability to decouple the light absorption length from the minority carrier diffusion length in porous structure makes it potentially more efficient. As a result, the porous GaP photoelectrode can be provided with high performance for photoelectrochemical water splitting. At the same time, the stability of porous structure was also illustrated in Fig. 6c, and the sample with etching time 45 s as an instance. The measurement condition of stability is the same as in the photocurrent measurement as shown in Fig. 6a. There is no obvious decrease of photocurrent, which indicates that the triangular pore arrays are stable in the PEC system.

In PEC water splitting, the water oxidation involving a four-electron transfer is normally more challenging than water reduction. The water oxidation performance of n-GaP under light irradiation was exhibited via photocurrent in Fig. 6d. The enhancement factor, which was defined as the photocurrent density of porous GaP over that of the bulk GaP [44], was over 10 under the 0.1 V compared to the RHE. It was noted that the enhancement factor was also exceeded 10 in range of  $-1.0$  to  $-0.5$  V compared to the Ag/AgCl reference electrode, as shown in Fig. 6d. In the bulk n-GaP, holes, as the minority carriers, have to traverse a long distance before reaching the bulk

surface to finish water oxidation, and most carriers have finished recombination during this process, which attributes the low efficiency of the photoelectrode. In comparison, the porous structure can capture the light to absorb efficiently along their entire depth, and holes can be effectively to collect over a short distance to promote water oxidation. Therefore, the porous photoelectrode displayed a much higher PEC activity than the bulk photoelectrode. Moreover, the onset potential of porous GaP is averagely less 50 mV than the bulk material as shown in Fig. 6d inset. The  $I$ - $V$  characteristics of porous GaP and bulk GaP electrode exhibited similar behavior as shown in Fig. 6a. The PEC performance of GaP improved as the etching time increased, and it reached the optimal capacity under the etching time of 45 s. In order to further prove this, IPCE was given in Fig. 7. The result suggested that the porous structure was more effectively in enhancing the efficiency. Optimizing the structure of the porous GaP could further improve the efficiency of the porous electrode.

The capability of the pore arrays on GaP to drive hydrogen production from water splitting under illumination at the solution with hole scavenger was demonstrated. We choose the sample etched with 30 s as an instance to compare with bulk material in the hydrogen production from photocatalytic water splitting. The mixture solution of 0.35 M  $\text{Na}_2\text{S}$  and 0.25 M  $\text{Na}_2\text{SO}_3$  was the sacrificial reagents in the hydrogen production of photocatalyst. The mechanism of hydrogen

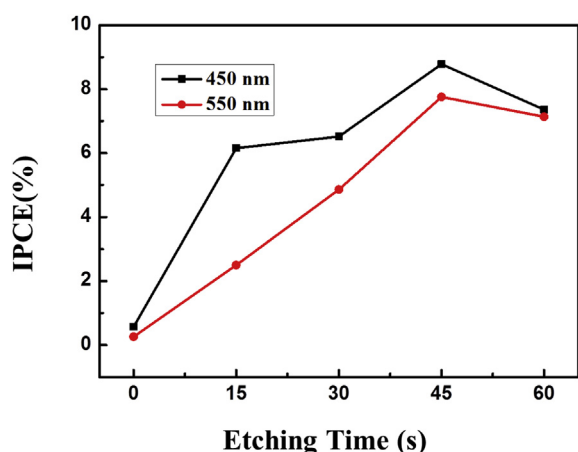
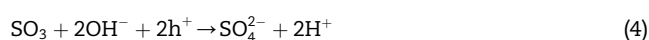
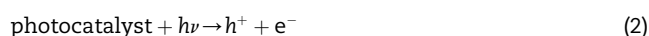


**Fig. 7** – IPCE plot of GaP with different etching time at 0.1 V vs RHE. The black and red curves are the corresponding wavelength of 450 nm and 550 nm. (For interpretation of the references to colour in this figure legend, the reader is referred to the web version of this article.)

production can be explained through the following equations (Eqs. (2)–(7)) [4,45]:



The mixture of  $\text{S}^{2-}/\text{SO}_3^{2-}$  has been used as electron donors and set to the water/semiconductor solution to enhance the

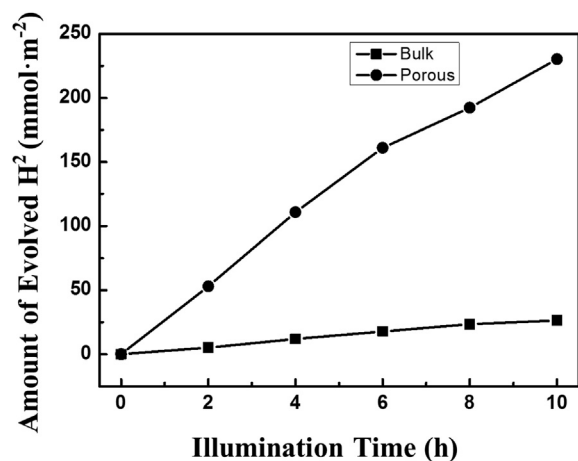


**Fig. 8** – Under illumination, the amount of evolved  $\text{H}_2$  for the GaP with the triangular pores and bulk material, respectively.

photocatalytic activity and stability for the production of hydrogen from water [46–51].

Fig. 8 showed that the hydrogen production of ordered porous GaP etched with 30 s was almost one order of magnitude higher than that of the bulk material in unit square. These results indicated the etched triangular pore arrays on GaP exhibited more photocatalytic activity. The enhancement of hydrogen production can be attributed to two effects related to the nature of the porous structure just like in the photocurrent measurement. In a control experiment conducted in the absence of GaP, hydrogen was not detected.

## Conclusions

In summary, triangular pore arrays on GaP have been obtained by electrochemical etching under high field. In comparison with bulk material, the photoresponse of this ordered porous GaP is enhanced. The PEC activity of the porous GaP can be further improved by optimizing the depth of pores, which is easily achieved by controlling the etching time. Due to this enhancement effect, the ordered porous GaP is higher efficient in absorbing light for driving water splitting. The significant improvement of hydrogen production indicates that the porous structure can decouple the light absorption length and increase the charge carrier collection. Therefore, we conclude that the application of the porous structure photoelectrode is an effective strategy for solving the carrier collection limitation of GaP in PEC performance. Moreover, ordered porous GaP can be used as a promising photocatalyst to drive water splitting.

## Acknowledgments

This work was supported by National Major Basic Research Project of 2012CB934302, National 863 Program 2011AA050518, the Natural Science Foundation of China (Grant nos. 11174197 and 61234005).

## REFERENCES

- [1] Walter MG, Warren EL, McKone JR, Boettcher SW, Mi Q, Santor EA, et al. Solar water splitting cells. *Chem Rev* 2010;110:6646–73.
- [2] Fujishima A, Honda K. Electrochemical photolysis of water at a semiconductor electrode. *Nature* 1972;238:37–8.
- [3] Kudo A, Miseki Y. Heterogeneous photocatalyst materials for water splitting. *Chem Soc Rev* 2009;38:253–78.
- [4] Chen X, Shen S, Guo L, Mao SS. Semiconductor-based photocatalytic hydrogen generation. *Chem Rev* 2010;110:6503–70.
- [5] Bolton JR, Struckler SJ, Connolly JS. Limiting and realizable efficiencies of solar photolysis of water. *Nature* 1985;316:495–500.
- [6] Liu C, Sun J, Tang J, Yang P. Zn-doped p-type gallium phosphide nanowire photocathodes from a surfactant-free solution synthesis. *Nano Lett* 2012;12:5407–11.

- [7] Tomkiewicz M, Woodall JM. Photoassisted electrolysis of water by visible irradiation of a p-type gallium phosphide electrode. *Science* 1977;196:990–1.
- [8] Nozik AJ. p–n photoelectrolysis cells. *App Phys Lett* 1976;29:150–3.
- [9] Sun J, Liu C, Yang P. Surfactant-free, large-scale, solution-liquid-solid growth of gallium phosphide nanowires and their use for visible-light-driven hydrogen production from water reduction. *J Am Chem Soc* 2011;133:19,306–19,309.
- [10] Dasgupta NP, Yang P. Semiconductor nanowires for photovoltaic and photoelectrochemical energy conversion. *Front Phys*; 2013 Feb:1–14.
- [11] Hagedorn K, Collins S, Maldonado S. Preparation and photoelectrochemical activity of macroporous p-GaP(100). *J Electrochem Soc* 2010;157:D588–92.
- [12] Maiolo JR, Kayes BM, Filler MA, Putnam MC, Kelzenberg MD, Atwater HA, et al. High aspect ratio silicon wire array photoelectrochemical cells. *J Am Chem Soc* 2007;129:12346–7.
- [13] Yang F, Forrest SR. Photocurrent generation in nanostructured organic solar cells. *ACS Nano* 2008;2:1022–32.
- [14] Park JH, Kim S, Bard AJ. Novel carbon-doped TiO<sub>2</sub> nanotube arrays with high aspect ratios for efficient solar water splitting. *Nano Lett* 2006;6:24–8.
- [15] Maiolo JR, Atwater HA, Lewis NS. Macroporous silicon as a model for silicon wire array solar cells. *J Phys Chem C* 2008;112:6194–201.
- [16] Price MJ, Maldonado J. Macroporous n-GaP in Nonaqueous Regenerative Photoelectrochemical Cells. *J Phys Chem C* 2009;113:11988–94.
- [17] Wang G, Ling Y, Li Y. Oxygen-deficient metal oxide nanostructures for photoelectrochemical water oxidation and other applications. *Nanoscale* 2012;4:6682–91.
- [18] Su F, Wang T, Lv R, Zhang J, Zhang P, Lu J, et al. Dendritic Au/TiO<sub>2</sub> nanorod arrays for visible-light driven photoelectrochemical water splitting. *Nanoscale* 2013;5:9001–9.
- [19] Osterloh F. Inorganic nanostructures for photoelectrochemical and photocatalytic water splitting. *Chem Soc Rev* 2013;42:2294–320.
- [20] Ern  BH, Vanmaekelbergh D, Kelly JJ. Morphology and strongly enhanced photoresponse of GaP electrodes made porous by anodic etching. *J Electrochem Soc* 1996;143:305–14.
- [21] Ricci PC, Salis M, Anedda A. A model for pore growth in anodically etched gallium phosphide. *J Appl Phys* 2005;97:113522.
- [22] Shen YC, Hon MH, Leu IC, Teoh LG. Morphological characterization of porous GaP prepared by electrochemical etching. *Appl Phys A* 2010;98:429–34.
- [23] Wloka J, Schmuki P. Morphology of porous n-GaP anodically formed in different mineral acids. *J Electroceram* 2006;16:23–8.
- [24] M ller K, Wloka J, Schmuki P. Novel pore shape and self-organization effects in n-GaP(111). *J Solid State Electrochem* 2009;13:807.
- [25] Wloka J, M ller K, Schmuki P. Pore morphology and self-organization effects during etching of n-type GaP(100) in bromide solutions. *Electrochem Solid-State Lett* 2005;8:B72–5.
- [26] Tjerkstra RW, G mez Rivas J, Vanmaekelbergh D, Kelly JJ. Porous GaP multilayers formed by electrochemical etching. *Electrochem Solid-State Lett* 2002;5:G32–5.
- [27] Tiginyanu IM, Kravetsky IV, Monecke J, Cordts W, Marowsky G, Hartnagel HL. Semiconductor sieves as nonlinear optical materials. *Appl Phys Lett* 2000;77:2415–7.
- [28] Hoang S, Guo S, Hahn NT, Bard AJ, Mullins CB. Visible light driven photoelectrochemical water oxidation on nitrogen-modified TiO<sub>2</sub> nanowires. *Nano Lett* 2012;12:26–32.
- [29] Tjerkstra RW. Electrochemical formation of porous GaP in aqueous HNO<sub>3</sub>. *Electrochem Solid-State Lett* 2006;9:C81–4.
- [30] F ll H, Langa S, Carstensen J, Christophersen M, Tiginyanu IM. Pores in III–V semiconductors. *Adv Mater* 2003;15:183–98.
- [31] Tomioka K, Adachi S. Structural and photoluminescence properties of porous GaP formed by electrochemical etching. *J Appl Phys* 2005;98:073511.
- [32] Langa S, Tiginyanu IM, Monaco E, F ll H. Porous II–VI vs. porous III–V semiconductors. *Phys Status Solidi C* 2011;8:1792–6.
- [33] Landa S, Carstensen J, Christophersen M, Steen K, Frey S, Tiginyanu IM, et al. Uniform and nonuniform nucleation of pores during the anodization of Si, Ge, and III–V semiconductors. *J Electrochem Soc* 2005;152:C525–31.
- [34] Stevens-Kalceff MA, Tiginyanu IM, Langa S, F ll H, Hartnagel HL. Correlation between morphology and cathodoluminescence in porous GaP. *J Appl Phys* 2001;89:2560–5.
- [35] Hwang YJ, Boukai A, Yang P. High density n-Si/n-TiO<sub>2</sub> core/shell nanowire arrays with enhanced photoactivity. *Nano Lett* 2009;9:410–5.
- [36] Kayes BM, Atwater HA, Lewis NS. Comparison of the device physics principles of planar and radial p–n junction nanorod solar cells. *J Appl Phys* 2005;97:114302.
- [37] Tan MX, Kenyon CN, Kr ger O, Lewis NS. Behavior of Si photoelectrodes under high level injection conditions. 1. Steady-state current–voltage properties and quasi-fermi level positions under illumination. *J Phys Chem B* 1997;101:2830–9.
- [38] Lewis NS. Mechanistic studies of light-induced charge separation at semiconductor/liquid interfaces. *Acc Chem Res* 1990;23:176–83.
- [39] Lewis NS. Chemical control of charge transfer and recombination at semiconductor photoelectrode surfaces. *Inorg Chem* 2005;44:6900–11.
- [40] Rosenbluth ML, Lieber CM, Lewis NS. 630 mV open circuit voltage, 12% efficient n-Si liquid junction. *Appl Phys Lett* 1984;45:423–5.
- [41] Yang X, Du C, Liu R, Xie J, Wang D. Balancing photovoltage generation and charge-transfer enhancement for catalyst-decorated photoelectrochemical water splitting: a case study of the hematite/MnO<sub>x</sub> combination. *J Catal* 2013;304:86–91.
- [42] Oh I, Kye J, Hwang S. Enhanced photoelectrochemical hydrogen production from silicon nanowire array photocathode. *Nano Lett* 2012;12:298–302.
- [43] Ern  BH, Vanmaekelbergh D, Kelly JJ. Porous etching: a means to enhance the photoresponse of indirect semiconductors. *Adv Mater* 1995;7:739–42.
- [44] Li Y, Takata T, Cha D, Takanabe K, Minegishi T, Kubota J, et al. Vertically aligned Ta<sub>3</sub>N<sub>5</sub> nanorod arrays for solar-driven photoelectrochemical water splitting. *Adv Mater* 2013;25:125–31.
- [45] Bao N, Shen L, Takata T, Domen K. Self-templated synthesis of nanoporous CdS nanostructures for highly efficient photocatalytic hydrogen production under visible light. *Chem Mater* 2008;20:110–7.
- [46] Yan H, Yang J, Ma G, Wu G, Zong X, Lei Z, et al. Visible-light-driven hydrogen production with extremely high quantum efficiency on Pt–PdS/CdS photocatalyst. *J Catal* 2009;266:165–8.
- [47] Inue T, Watanabe T, Fujishima A, Honda K, Kohayakawa K. Suppression of surface dissolution of CdS photoanode by reducing agents. *J Electrochem Soc* 1977;124:719–22.
- [48] Koriche N, Bouguelia A, Trari M. Photocatalytic hydrogen production over new oxide CuLaO<sub>2.62</sub>. *Int J Hydrogen Energy* 2006;31:1196–203.

- 
- [49] Shen S, Guo L, Chen X, Ren F, Mao SS. Effect of Ag<sub>2</sub>S on solar-driven photocatalytic hydrogen evolution of nanostructured CdS. *Int J Hydrogen Energy* 2010;35:7110–5.
- [50] Zhang K, Jing D, Chen Q, Guo L. Influence of Sr-doping on the photocatalytic activities of CdS–ZnS solid solution photocatalysts. *Int J Hydrogen Energy* 2010;35:2048–57.
- [51] Xu M, Zai J, Yuan Y, Qian X. Band gap-tunable (CuIn)<sub>x</sub>Zn<sub>2(1-x)</sub>S<sub>2</sub> solid solutions: preparation and efficient photocatalytic hydrogen production from water under visible light without noble metals. *J Mater Chem* 2012;22:23,929–23,934.